Large and unexpected enrichment in stratospheric $^{16}O^{13}C^{18}O$ and its meridional variation

Laurence Y. Yeung[a,1,2], Hagit P. Affek[b,1], Katherine J. Hoag[c,3], Weifu Guo[e,4], Aaron A. Wiegel[d], Elliot L. Atlas[f], Sue M. Schauffler[g], Mitchio Okumura[a], Kristie A. Boering[c,d], and John M. Eiler[e]

Divisions of [a]Chemistry and Chemical Engineering and [e]Geological and Planetary Sciences, California Institute of Technology, Pasadena, CA 91125; [b]Department of Geology and Geophysics, Yale University, New Haven, CT 06511; Departments of [c]Chemistry and [d]Earth and Planetary Science, University of California, Berkeley, CA 94720; [f]Division of Marine and Atmospheric Chemistry, University of Miami, Miami, FL 33149; and [g]National Center for Atmospheric Research, Boulder, CO 88307

Edited by Mark H. Thiemens, University of California at San Diego, La Jolla, CA, and approved May 26, 2009 (received for review March 16, 2009)

The stratospheric CO_2 oxygen isotope budget is thought to be governed primarily by the $O(^1D)+CO_2$ isotope exchange reaction. However, there is increasing evidence that other important physical processes may be occurring that standard isotopic tools have been unable to identify. Measuring the distribution of the exceedingly rare CO_2 isotopologue $^{16}O^{13}C^{18}O$, in concert with ^{18}O and ^{17}O abundances, provides sensitivities to these additional processes and, thus, is a valuable test of current models. We identify a large and unexpected meridional variation in stratospheric $^{16}O^{13}C^{18}O$, observed as proportions in the polar vortex that are higher than in any naturally derived CO_2 sample to date. We show, through photochemical experiments, that lower $^{16}O^{13}C^{18}O$ proportions observed in the midlatitudes are determined primarily by the $O(^1D)+CO_2$ isotope exchange reaction, which promotes a stochastic isotopologue distribution. In contrast, higher $^{16}O^{13}C^{18}O$ proportions in the polar vortex show correlations with long-lived stratospheric tracer and bulk isotope abundances opposite to those observed at midlatitudes and, thus, opposite to those easily explained by $O(^1D)+CO_2$. We believe the most plausible explanation for this meridional variation is either an unrecognized isotopic fractionation associated with the mesospheric photochemistry of CO_2 or temperature-dependent isotopic exchange on polar stratospheric clouds. Unraveling the ultimate source of stratospheric $^{16}O^{13}C^{18}O$ enrichments may impose additional isotopic constraints on biosphere–atmosphere carbon exchange, biosphere productivity, and their respective responses to climate change.

clumped isotopes | CO_2 | mesosphere | polar vortex | stratosphere

Predicting future CO_2 concentrations and carbon cycle–climate feedbacks depends on accurately quantifying the contributions from the sources and sinks governing the global carbon budget and how they may change over time. The bulk stable isotope composition of CO_2 (i.e., its $^{13}C/^{12}C$, $^{18}O/^{16}O$ and $^{17}O/^{16}O$ ratios) plays an important role in constraining this budget (ref. 1 and references therein). In the stratosphere, the oxygen isotopic composition of CO_2 is thought to be modified by oxygen isotope exchange reactions with $O(^1D)$ generated by ozone photolysis (2), whereas in the troposphere it is controlled by isotope exchange reactions with liquid water in the oceans, soils, and plant leaves (3). The interplay between stratospheric and tropospheric isotope exchange reactions, in principle, could allow the relative abundances of $^{12}C^{16}O_2$, $^{16}O^{12}C^{18}O$, and $^{16}O^{12}C^{17}O$ isotopologues to be used as tracers for gross biosphere productivity (4, 5), but the stratospheric CO_2 photochemical system is still underconstrained, and our understanding of it is incomplete.

Discrepancies between laboratory and stratospheric measurements (6–8) have prompted questions about whether the $O(^1D)+CO_2$ isotope exchange reaction acts alone on stratospheric CO_2 or whether other photochemical (9) or dynamical (10) processes significantly affect the stable isotopologue distribution in CO_2. Stratospheric oxygen isotope covariations in CO_2 (8, 11, 12) consistently differ from those found in laboratory experiments simulating stratospheric photochemistry (6, 13–16), and the origin of this disagreement is still uncertain because bulk stable isotope measurements (i.e., of $\delta^{13}C$, $\delta^{17}O$, and $\delta^{18}O$ values) alone cannot differentiate extrinsic effects [e.g., $O(^1D)$ isotope composition] from intrinsic (i.e., photolytic or kinetic isotope) effects on the isotope composition of stratospheric CO_2. Additional constraints arising from the analysis of multiply-substituted isotopologues of CO_2 can provide sensitivities to these processes (17–20). To investigate stratospheric CO_2 chemistry, we examine here the proportions of the $^{16}O^{13}C^{18}O$ (reported as a Δ_{47} value; see *Materials and Methods*) in stratospheric CO_2 and in laboratory kinetics experiments.

Field and Laboratory Results

Six samples of stratospheric CO_2 collected from the NASA ER-2 aircraft during the 1999/2000 Arctic winter Stratospheric Aerosol and Gas Experiment III (SAGE III) Ozone Loss and Validation Experiment (SOLVE) campaign (21) and 6 additional CO_2 samples collected from a balloon flight from Fort Sumner, NM, on September 29, 2004 were analyzed for bulk stable isotope compositions and Δ_{47} values (see *Materials and Methods* and Table 1). The stratospheric samples display Δ_{47} values both higher and more variable than those exhibited by tropospheric air at the surface, which has an average Δ_{47} value of $0.92 \pm 0.01‰$ in remote regions (Cape Grim, Tasmania and Barrow, Alaska) (18). The high-latitude (>57°N) stratospheric samples, in particular, are significantly more enriched in Δ_{47} than any material analyzed before in nature (see Fig. 1 and refs. 18 and 20). At high latitudes, Δ_{47} varies strongly and increases monotonically with decreasing mixing ratios of long-lived trace gases that have tropospheric sources and stratospheric sinks, such as N_2O and CH_4. At midlatitudes, Δ_{47} varies relatively little and shows correlations with trace-gas mixing ratios having the opposite sign of those observed at high latitudes [e.g., Fig. 2*A*; see supporting information (SI)]. Using the correlation between simultaneously measured N_2O mixing ratios and potential tem-

Author contributions: L.Y.Y., H.P.A., M.O., and J.M.E. designed research; L.Y.Y., H.P.A., K.J.H., W.G., E.L.A., S.M.S., and K.A.B. performed research; L.Y.Y., H.P.A., W.G., and A.A.W. performed modeling; L.Y.Y., H.P.A., K.J.H., A.A.W., K.A.B., and J.M.E. contributed new reagents/analytic tools; L.Y.Y., H.P.A., W.G., A.A.W., M.O., K.A.B., and J.M.E. analyzed data; and L.Y.Y., H.P.A., W.G., A.A.W., K.A.B., and J.M.E. wrote the paper.

The authors declare no conflict of interest.

This article is a PNAS Direct Submission.

[1]L.Y.Y. and H.P.A. contributed equally to this work.

[2]To whom correspondence should be addressed. E-mail: lyeung@caltech.edu.

[3]Present address: United States Environmental Protection Agency (Region 9), San Francisco, CA 94105.

[4]Present address: Geophysical Laboratory, Carnegie Institution of Washington, Washington, DC 20015.

This article contains supporting information online at www.pnas.org/cgi/content/full/0902930106/DCSupplemental.

Table 1. Stratospheric air sample data

Air type*	Sample name	Altitude, km	Latitude, °N	N_2O, ppbv	CH_4, ppbv	θ, K	$\delta^{13}C$, ‰	$\delta^{18}O$, ‰	$\Delta^{17}O$, ‰	Δ_{47}, ‰
ER-2 samples										
V	20000312(25)1120	19.33	79.2	111.5	948	443.61	−8.11	44.55	5.76	1.614
V	20000131(30)1001	19.85	73.5	142.1	1,066	448.08	−8.08	43.62	4.38	1.555
V	20000203(10)1173	17.63	70.4	192.8	1,250	409.37	−8.06	43.06	3.69	1.436
VE	20000127(5)1060	19.45	57.7	227.6	1,385	445.10	−8.07	42.79	2.45	1.233
M	20000106(30)1169	19.40	29.3	256.4	1,495	467.43	−8.08	42.50	2.13	1.071
M	20000111(25)2021	11.40	43.5	307.9	1,726	358.26	−8.06	40.98	0.18	1.075
Balloon samples										
M	1-A010-R (2035)	33.34	34.5	54.0	835	931.14	−8.07	45.14	6.46	0.976
M	3-A01-R (1141)	32.22	34.6	56.7	843	896.15	−7.99	45.44	6.29	0.923
M	7-A026-R (1057)	29.26	34.6	92.1	957	778.08	−8.07	44.98	6.12	0.912
M	5-A013-R (2079)	30.78	34.6	77.8	913	861.84	−8.03	45.14	5.91	0.913
M	8-A017-E (1113)	28.73	34.6	107.9	1,014	757.89	−8.04	44.79	5.00	1.004
M	10-A022-E (1186)	27.27	34.6	155.9	1,176	709.67	−8.03	44.09	4.26	0.916

*Air type is abbreviated as V, vortex; VE, vortex edge; and M, midlatitude, based on N_2O/θ correlations, where θ is potential temperature in Kelvin.

perature (22), we found that the high-latitude samples were collected in either inner polar vortex air (3 samples) or vortex edge air (1 sample). Thus, differences in the sign and magnitude of Δ_{47} variations with N_2O mixing ratio in the 2 subsets of samples are presumably due to differences between vortex and nonvortex processes. In contrast to these Δ_{47} trends, covariations of $\Delta^{17}O$ with $\delta^{18}O$ and mixing ratios of long-lived trace gases for our midlatitude samples resemble those of our polar vortex samples (or show the expected differences for slightly shorter-lived tracers, e.g., CFC-11) and also those reported in earlier studies of high-latitude (10, 11) and polar vortex air (23) (see SI). This suggests that Δ_{47} records a process to which $\Delta^{17}O$ is not sensitive.

To gain further insight into the correlations we observed between Δ_{47}, $\Delta^{17}O$, and $\delta^{18}O$, we conducted several laboratory photochemistry experiments. Enrichments of $\Delta^{17}O$ and $\delta^{18}O$ in stratospheric CO_2 are generally understood to arise from isotope exchange with $O(^1D)$, which is produced by photolysis of ^{17}O- and ^{18}O-enriched stratospheric ozone (2, 24), but the kinetics of the isotope exchange reactions for multiply-substituted isotopologues of CO_2, and their effects on Δ_{47}, have not yet been explored. Changes in Δ_{47} caused by these reactions should principally reflect relative changes in $^{16}O^{13}C^{18}O$ and $^{16}O^{12}C^{18}O$ abundances because the ^{13}C composition is not affected by isotope exchange with $O(^1D)$; variations in $^{17}O^{12}C^{18}O$ and $^{13}C^{17}O_2$ abundances will change Δ_{47} more subtly (see SI). Thus, reactions 1 and 2 are most relevant.

$$^{18}O(^1D) + {}^{12}C^{16}O_2 \rightarrow {}^{18}O^{12}C^{16}O_2^* \rightarrow {}^{16}O + {}^{16}O^{12}C^{18}O \quad [1]$$

$$^{18}O(^1D) + {}^{13}C^{16}O_2 \rightarrow {}^{18}O^{13}C^{16}O_2^* \rightarrow {}^{16}O + {}^{16}O^{13}C^{18}O \quad [2]$$

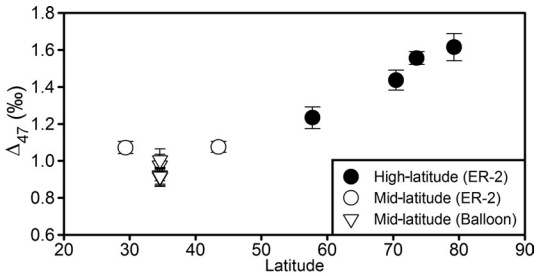

Fig. 1. Meridional variation of Δ_{47} measured in stratospheric samples. Typical values in the troposphere are $\Delta_{47} \approx 0.9$‰. Error bars show 2σ standard errors.

Statistical partitioning of isotope exchange products, through a process governed by random chance such that $^{18}O(^1D)$ has a 2/3 probability of being incorporated into the product CO_2, would drive the CO_2 isotopologues toward a stochastic distribution (i.e., $\Delta_{47} = 0$). If any one (or more) of the isotope exchange reactions does not partition products statistically, however, Δ_{47} can increase (e.g., if $^{18}O(^1D)$ exchanges isotopes with $^{13}C^{16}O_2$ more readily than with $^{12}C^{16}O_2$) or decrease accordingly.

Two sets of laboratory experiments were conducted. First, the relative rates of reactions 1 and 2 were probed directly to obtain the $^{13}C/^{12}C$ kinetic isotope effect (KIE) for the $^{18}O(^1D)+CO_2$ isotope exchange reaction at 300 K and 229 K. These experiments used pulsed photolysis of 97% $N_2{}^{18}O$ at 193 nm as a source of $^{18}O(^1D)$, and the extent of isotope exchange was minimized.

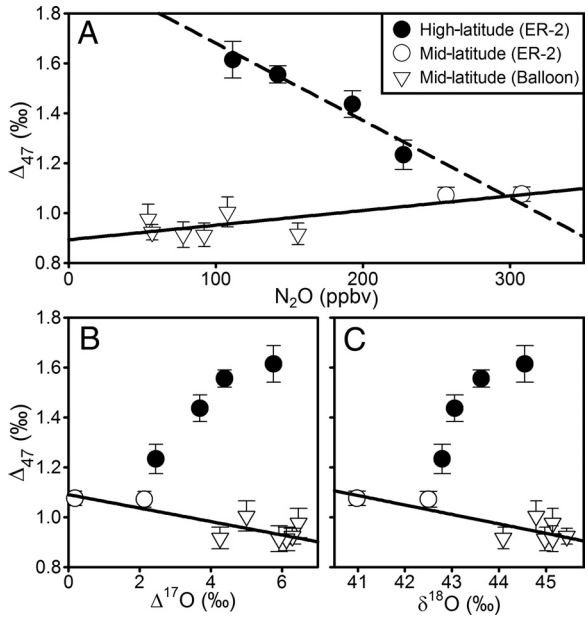

Fig. 2. Correlations between Δ_{47} and stratospheric tracers. (*A*), best-fit lines are shown for midlatitude (solid line) and high-latitude (dashed line) Δ_{47} vs. N_2O mixing ratio. Correlations between Δ_{47} and other tracers with tropospheric sources and stratospheric sinks are similar (see *SI*). (*B* and *C*) Best-fit lines of Δ_{47} vs. $\delta^{18}O$ (*B*) and Δ_{47} vs. $\Delta^{17}O$ (*C*) in midlatitude air, which are used to estimate the integrated effective isotopic composition of stratospheric $O(^1D)$ (see *$O(^1D)+CO^2$ Explains Midlatitude but Not Polar Vortex $^{16}O^{13}C^{18}O$ Variations* and *Materials and Methods*). Error bars show 2σ standard errors.

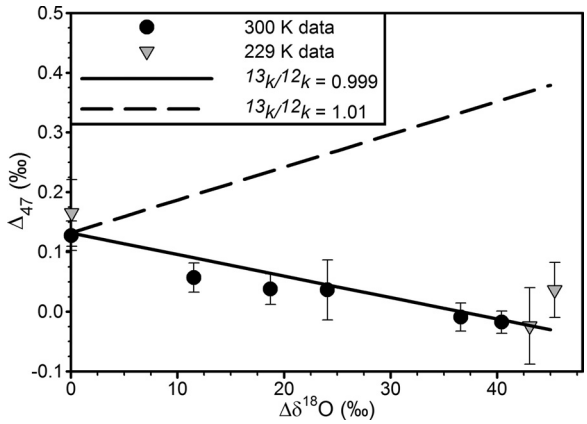

Fig. 3. Results of laboratory photochemical experiments. Changes in Δ_{47} vs. $\Delta\delta^{18}$O after pulsed UV photolysis at 300 K (circles) and 229 K (triangles) are shown. $\Delta\delta^{18}O = \delta^{18}O_{final} - \delta^{18}O_{initial}$. Also shown is the modeled Δ_{47} vs. $\Delta\delta^{18}$O dependence for $^{13}C/^{12}C$ KIE = $^{13}k/^{12}k$ = 0.999 and 1.01 (offset by Δ_{47} = +0.13‰ for clarity; the significance of this and of the slopes is discussed below and in *SI*). Error bars show 2σ standard errors.

They were performed in an excess of helium to probe a stratospherically relevant range of collision energies (see SI) because the reaction dynamics are sensitive to reactant collision energies (25). Second, we performed continuous irradiation experiments, using a mercury lamp, on mixtures of isotopically unlabeled O_2, O_3, and CO_2 as a function of different irradiation times to determine the cumulative effects of the $O_2/O_3/CO_2$ photochemical system on Δ_{47}.

In both sets of experiments, Δ_{47} of CO_2 decreases with increasing extent of photochemical isotope exchange, as measured by the change in $\delta^{18}O$ ($\Delta\delta^{18}O$; see Fig. 3) or $\Delta^{17}O$ of CO_2 (see SI), indicating the $O(^1D)+CO_2$ reaction does not selectively enrich $^{16}O^{13}C^{18}O$ relative to $^{16}O^{12}C^{18}O$. Furthermore, these results are consistent with the statistical partitioning of isotope exchange products; using the results from the ^{18}O-labeled experiments at 300 K and 229 K and a comprehensive kinetics model of the pulsed photolysis experiment, we calculate a $^{13}C/^{12}C$ KIE of 0.999 ± 0.001 (2σ est.), which is not significantly different from the KIE of 1.000 expected for statistical isotope exchange branching fractions and is quantitatively consistent with the results from the continuous irradiation experiments. Hence, our results are consistent with previous studies asserting that the $O(^1D)+CO_2$ isotope exchange products are partitioned statistically (14, 16, 25). In contrast, a $^{13}C/^{12}C$ KIE of ≈1.01 would be required to explain the high-latitude isotopic correlations shown in Fig. 2 *B* and *C* (see SI).

It is possible that the measured KIEs depend on reactant collision energies, which can have a nonthermal distribution in the stratosphere (26). Previous work has shown that the $O(^1D)+CO_2$ isotope exchange reaction occurs through 2 reaction channels whose branching ratio varies with collision energy (25):

$$O(^1D) + CO_2 \rightarrow O(^3P) + CO_2 \quad \textbf{[3a]}$$

$$\rightarrow O(^1D) + CO_2 \quad \textbf{[3b]}$$

Under typical stratospheric conditions, the channel shown as Reaction **3a** dominates. However, the contribution from the nonquenching isotope exchange channel, shown as Reaction **3b**, increases significantly with reactant collision energy (25). Because the KIEs for the channels shown as Reactions **3a** and **3b** may differ, both between the 2 channels and as a function of collision energy (27), the overall KIE in the lab or atmosphere may also depend on these parameters. High-collision-energy (no buffer gas) experiments, which tip the 3a/3b branching ratio toward the reaction shown as Reaction **3b**, were performed to test this hypothesis. Similar to the low-collision-energy experiments described above, these experiments also showed depletions in Δ_{47} as the extent of photochemical isotope exchange increased, with no significant change in the Δ_{47} vs. $\Delta\delta^{18}O$ trend (see SI). This indicates that the KIE we report is relatively insensitive to the 3a/3b branching ratio. Still, more experimental studies will be required to quantify these channel-specific KIEs.

$O(^1D)+CO_2$ Explains Midlatitude but Not Polar Vortex $^{16}O^{13}C^{18}O$ Variations

We conclude that intrinsic isotope effects in $O(^1D)+CO_2$ isotope exchange cannot produce the elevated values of Δ_{47} observed in stratospheric polar vortex air. Instead, the statistical partitioning of isotope exchange products in the $O(^1D)+CO_2$ reaction drives the isotopic composition of CO_2 toward a stochastic distribution, thus decreasing Δ_{47}. Indeed, the midlatitude observations show evidence for decreasing Δ_{47} with increasing extent of photochemical isotope exchange (see Fig. 2 *B* and *C*). As photochemical isotope exchange approaches completion (the unlikely, but instructive case in which all of the oxygen atoms in CO_2 have been exchanged), the $\Delta^{17}O$ and $\delta^{18}O$ of CO_2 will approach the $\Delta^{17}O$ and $\delta^{18}O$ of $O(^1D)$ because the size of the oxygen reservoir is >500 times that of CO_2. Concurrently, the distribution of stable isotopes will become increasingly random, so the Δ_{47} value of CO_2 will approach zero. The slope of this approach, then, reflects the integrated effective isotope composition of $O(^1D)$ with which the CO_2 molecules in the air samples have exchanged since entering the stratosphere; it is possible, however, that other terms in the stratospheric CO_2 budget (e.g., CO oxidation) may, more subtly, change the isotopic composition of CO_2 and thus the isotopic composition of $O(^1D)$ one would infer from such a trend. Using a box model and the midlatitude observations, we estimate $\Delta^{17}O = 80.6^{+59.7}_{-24.1}$‰ and $\delta^{18}O = 98.0^{+43.7}_{-17.1}$‰ (2$\sigma$ est.) as values for the integrated effective isotopic composition of $O(^1D)$, which is consistent with ozone photolysis being the primary $O(^1D)$ source in the stratosphere. Although the $\delta^{18}O$ of $O(^1D)$ we calculate is similar to that found in low- and midlatitude stratospheric ozone, $\Delta^{17}O$ is larger, on average, by 35‰ (28). This is expected because $\Delta^{17}O$ enrichments in ozone are concentrated at terminal atom positions (29); when ozone is photolyzed to $O(^1D)$ and O_2, one of the terminal atoms is ejected (30), elevating the proportion of heavy oxygen isotopes in $O(^1D)$. The uncertainty bounds reported here reflect spatial and temporal variations in $O(^1D)$ isotope composition expected to be caused by variations in ozone concentrations, temperature, pressure, actinic flux, and various mass-dependent kinetic and photolytic isotope effects that depend on these variables.

Having experimentally excluded intrinsic isotope effects in the $O(^1D)+CO_2$ isotope exchange reaction as the source of high stratospheric Δ_{47} in polar vortex air, we consider the possible effects of other gas-phase stratospheric processes on the CO_2 isotopologue budget. CO is produced in the stratosphere by CH_4 oxidation and destroyed with an e-folding time of ≈2–3 months by reaction with OH radicals to form CO_2. We estimate that up to 0.9 ppmv CO_2 could be derived from CH_4 oxidation in our samples based on the difference between the observed CH_4 concentrations (Table 1) and the average CH_4 concentration in air entering the stratosphere from the troposphere (1.7 ppmv). $^{12}C/^{13}C$ KIEs for CH_4+OH, $CH_4+O(^1D)$, and CH_4+Cl of 1.004, 1.01, and 1.07, respectively (31), should yield ^{13}C-depleted CH_3 radicals at all latitudes, particularly in the polar vortex, where Cl levels are elevated. CH_3 radicals then undergo several rapid oxidation steps to form formaldehyde (CH_2O). Isotope effects in CH_2O photolysis to form CO also favor the light isotopologues (32). These isotope effects, combined with expected ^{13}C com-

positions for stratospheric CH_4 in these samples ($\delta^{13}C = -47$ to $-35‰$) should produce CO that is depleted in ^{13}C relative to background stratospheric CO_2. Small inverse $^{12}C/^{13}C$, $^{16}O/^{18}O$, and $^{16}C/^{17}O$ KIEs (i.e., <1) in the reaction CO+OH to form CO_2 at low pressures (33) imply that, in principle, CO+OH reactions could increase Δ_{47} values in the product CO_2, whereas at higher pressures, the CO+OH reaction yields ^{13}C-, ^{18}O-, and ^{17}O-depleted CO_2 (34). Ultimately, however, the size of Δ_{47} values in the up to 0.9 ppmv CO_2 derived from CH_4 oxidation would likely be orders of magnitude too small to increase Δ_{47} values significantly in the other ≈365 ppmv of background stratospheric CO_2. A possibility remains that unusual timing in the competition between oxidation and photolysis of species in the polar vortex, combined with unexpectedly large carbon and oxygen KIEs in some Cl and Br reactions (e.g., Br + CH_2O; see ref. 35) or other gas-phase processes might be responsible for the midlatitude–polar vortex differences in Δ_{47} given the large differences in Cl and Br concentrations in polar vortex vs. midlatitude air, but this seems unlikely in light of the known chemistry and KIEs.

Stratospheric mixing of 2 or more reservoirs of isotopically distinct CO_2 could also produce higher Δ_{47} values in the resulting mixtures because mixing 2 isotopically distinct CO_2 reservoirs can produce nonstochastic abundances of multiply-substituted isotopologues. This nonlinear dependence of Δ_{47} on mixing arises because the reference against which the measured $^{47}CO_2/^{44}CO_2$ ratio is compared (i.e., the mixture's stochastic distribution) is not constant upon mixing; this reference is defined by, and therefore varies with, the bulk stable isotope ratios of that mixture. In contrast, the references used in bulk stable isotope measurements are external standards whose values are constant (e.g., VSMOW), so the bulk isotope ratios vary linearly with mixing (see SI). The degree of nonlinearity in Δ_{47} is a function of the differences in bulk isotopic composition between the mixing end-member reservoirs and their mixing fractions (17, 19). We calculate that bulk isotope compositions of the 2 CO_2 reservoirs must differ in $\delta^{18}O$ and/or $\delta^{13}C$ by orders of magnitude not previously observed in the stratosphere to generate Δ_{47} enrichments of ≈0.7‰ observed in polar vortex samples.

Effects of Mesospheric and Heterogeneous Chemistry

Physical or chemical processes in the mesosphere may yield extreme isotopic enrichments in CO_2 or CO such that subsidence of mesospheric air into the 1999/2000 stratospheric polar vortex (36) could explain the observed meridional variation in Δ_{47}. Here, we consider 3 mesospheric processes that have been previously studied in other contexts: Gravitational separation of upper atmospheric air, UV photolysis of O_2, and UV photolysis of CO_2. Gravitational separation can concentrate heavy isotopologues of CO_2 into the lower mesosphere (37), but the isotopic enrichments we calculate, based on the expression reported by Craig et al. (38), are insufficient to generate significant Δ_{47} changes (see SI). Alternatively, isotope effects in the photolysis of O_2 by short-wavelength UV radiation in the upper mesosphere might lead to unusually enriched CO_2. Liang et al. (24) predicted recently that differences in photolysis cross-sections between light and heavy isotopologues of O_2 in the narrow solar Lyman-α region (121.6 nm) may result in a population of mesospheric $O(^1D)$ enormously enriched in ^{17}O and ^{18}O. This extreme enrichment in $O(^1D)$ could then be transferred to mesospheric CO_2 through the $O(^1D)+CO_2$ isotope exchange reaction. CO_2 photolysis in the mesosphere to form CO, followed by oxidation of that CO by OH in the polar vortex, might also significantly affect the Δ_{47} values of CO_2 in the polar vortex.

To evaluate the effects of ^{17}O- and ^{18}O-enriched mesospheric CO_2 mixing into the stratospheric polar vortex, we constructed a 3-component mixing model that included air mass contributions from the troposphere, stratosphere, and mesosphere. Each polar vortex datum (i.e., with unique $\Delta^{17}O$, $\delta^{18}O$, and Δ_{47} values) was fit individually because of the presence of mesospheric filaments in the polar vortex (36) and consequent heterogeneity in the mixing fraction and end-member isotopic composition between samples. Using the mesospheric ^{18}O and ^{17}O enrichments in CO_2 mixing end-member suggested by Liang et al. (i.e., $\delta^{18}O = 10{,}603‰$, $\delta^{17}O = 3{,}149‰$, and $\Delta_{47} = 0$; see *Materials and Methods*), we were unable to reproduce the polar vortex data in both bulk isotope compositions and Δ_{47} simultaneously. Only after $\delta^{18}O$ and $\delta^{17}O$ of the mesospheric CO_2 end-member were increased an additional 10-fold (i.e., $\delta^{18}O \approx 10^5‰$ and $\delta^{17}O \approx 10^4‰$) were the Δ_{47}-$\delta^{18}O$-$\Delta^{17}O$ systematics of the polar vortex samples reproduced. No laboratory measurements of the isotopic fractionations in O_2 due to Lyman-α photolysis are available to compare with this prediction, however. Furthermore, we note that the $O(^1D)+CO_2$ reaction may not necessarily partition products statistically (i.e., drive $\Delta_{47} \rightarrow 0$) in the mesosphere, as we assumed here, because the average collision energy there is higher than in the stratosphere.

In principle, measurements of the isotopic composition of mesospheric CO should constrain the isotopic composition of mesospheric CO_2 downwelling into the polar vortex. Large elevations in CO above background stratospheric levels, observed at high altitudes in the polar vortex (36), are due to CO_2 photolysis in the mesosphere and subsequent transport to the stratosphere, so the isotopic composition of CO in these cases should reflect that of the mesospheric CO_2 population and any fractionations arising from CO_2 photolysis there. The bulk isotopic composition in mesospheric CO_2 predicted by our 3-component mixing model (e.g., tens of percentage in ^{18}O-atom abundance, or 100 times natural abundance) would result in isotopic enrichments in mesospheric CO that are detectable with remote-sensing spectrometers because CO_2 photolysis isotope effects are expected to be much smaller in magnitude. For example, Bhattacharya et al. (9) measured fractionations of ≈100‰ in ^{17}O and ^{18}O in their UV-photolysis experiments; CO_2-photolysis fractionation in the mesosphere could be larger, but the wavelength dependence of these across the actinic spectrum is difficult to estimate because the physical origin of the laboratory fractionations is not understood (see SI). Remote-sensing measurements by the Jet Propulsion Laboratory MkIV Fourier-transform spectrometer, however, does not show hundredfold enrichments in ^{18}O of mesospheric CO observed downwelling to 30-km altitude in the polar vortex (G. C. Toon, personal communication). On the basis of this observation, mesospheric CO_2 does not appear to possess oxygen isotopic enrichments of sufficient size to produce high Δ_{47} values in the polar vortex upon mixing with stratospheric air masses, although the long path length and consequent averaging over mesospheric filaments and background stratospheric air of the MkIV instrument will dilute any mesospheric signal. Additional remote sensing of CO and/or CO_2 isotopologue abundances in the mesosphere is thus needed to constrain this hypothesis.

Once in the stratosphere, mesospheric CO will be oxidized by OH to produce CO_2 in the polar vortex. Oxidation of this CO could, in principle, contribute to the large polar vortex values of Δ_{47} in CO_2 observed because: (*i*) CO mixing ratios as large as 10 ppmv have been observed (36) in mesospheric filaments in the stratosphere (a thousandfold higher than background stratospheric CO abundances in the polar vortex), (*ii*) the known KIEs for the CO+OH reaction (33, 34) are expected to favor formation of $^{13}C^{18}O$-containing CO_2 molecules in the stratosphere, and (*iii*) the lifetime of CO with respect to oxidation is several months and is therefore not immediately quantitative. Measurements of the $^{13}C^{18}O+OH$ vs. $^{12}C^{18}O+OH$ KIE by Feilberg et al. (34) at 298 K and 1 atm suggest that the oxidation of mesospheric CO alone could account for elevated Δ_{47} stratospheric polar vortex. Measurements of all of the relevant KIEs of CO+OH reaction at stratospheric temperatures and pressures and a

model of the oxidation of mesospheric CO in the stratospheric polar vortex will be required to evaluate the impact of this mechanism quantitatively.

Finally, we consider the potential role stratospheric particles could play in the stratospheric CO_2 isotopic budget. Oxygen isotope exchange on particle surfaces could drive the population of CO_2 toward isotopic equilibrium by catalyzing CO_2–CO_2 isotope exchange reactions (e.g., $^{16}O^{12}C^{18}O + {}^{13}C^{16}O_2 \rightleftharpoons {}^{12}C^{16}O_2 + {}^{16}O^{13}C^{18}O$) that are too slow to occur in the gas phase under stratospheric conditions. Zero-point energy isotope effects dominate in these reactions at equilibrium, driving the Δ_{47} value toward its equilibrium value at a given temperature. We calculate that Δ_{47} adopts a value of 1.6‰ if 70% of the CO_2 molecules achieve isotopic equilibrium at temperatures coincident with PSC formation, ≈190 K (39), which occurs primarily in the polar vortex. Thus, in principle, particle-catalyzed equilibration of CO_2, perhaps via CO_2 hydration reactions in quasiliquid films at the surface of ice particles (40), could produce the observed polar vortex Δ_{47} values. Bulk isotopic compositions would be little affected by these isotope exchange reactions, consistent with the data presented in Table 1 and Fig. 2, if the catalyst reservoir (e.g., liquid water layers on a surface) is much smaller than the CO_2 reservoir; CO_2 would impart its bulk isotopic composition on the catalyst, whereas the multiply-substituted isotopologue distribution in CO_2, which is insensitive to the isotopic composition of the catalyst, approaches that at isotopic equilibrium. However, CO_2–liquid water isotope exchange may not occur quickly enough at low temperatures and low pH to be the relevant process. Experiments measuring the rate of CO_2 isotope exchange reactions at laboratory PSC– and sulfuric acid–air interfaces should determine the plausibility of this mechanism. Last, we note that, in order for this PSC-catalyzed isotope-exchange mechanism to explain the polar vortex Δ_{47} measurements, the mechanism must result in a strong anticorrelation with N_2O mixing ratios (Fig. 2*A*); this would imply that transport is fast compared with isotope exchange on the PSCs, whose distributions are highly variable in space and time in the polar vortex. Future 2D modeling efforts will examine whether such a mechanism remains consistent with the observations or whether transport and mixing of a mesospheric isotope signal into the polar vortex better explains the observed anticorrelation of Δ_{47} with N_2O.

Conclusions

The signature of a new process preserved in stratospheric $^{16}O^{13}C^{18}O$ proportions reveals that a second mechanism, in addition to the $O(^1D)+CO_2$ isotope exchange reaction, alters the isotopic composition of stratospheric CO_2 and thus the interpretation of its chemical and transport "history." This second mechanism, which elevates Δ_{47} values in the polar vortex, is likely of either mesospheric photochemical or heterogeneous origin. To constrain further the role of each of these mechanisms, isotopic fractionations due to broadband UV photolysis of O_2 and CO_2, the KIEs of the CO+OH reaction under stratospheric conditions, and the kinetics of CO_2 isotope equilibration on the surfaces of PSCs and other stratospheric aerosols need to be studied experimentally. Additionally, kinetic and photolysis-induced isotope effects that may affect CO and CO_2 should be incorporated into atmospheric models to quantify their contributions to both the bulk and multiply-substituted isotopologue budgets of stratospheric CO_2, whose influence on the isotopologue budgets of tropospheric CO_2 may be significant.

Materials and Methods

Air Sampling. SOLVE mission samples (January–March 2000, 29–79°N, 11–20 km) were collected as whole air samples (WAS) (41). CO_2 was then isolated from the ≈5-L STP of air by a combination of liquid N_2 and ethanol–dry ice traps, then separated into aliquots of 12–18 μmol of CO_2 each and sealed into glass ampoules. Balloon samples were collected by using a cryogenic whole-air sampler (CWAS) (September 29, 2004; 34.5°N, 103.6°W, 27–33 km) (42, 43) and purified and stored as above.

Isotopic Notation. $\delta^{18}O = (R^{18}_{sample}/R^{18}_{reference} - 1) \times 1{,}000$, where R^n is the abundance ratio of a rare isotope or isotopologue of mass n to its most abundant analogue, e.g., $R^{18} = [^{18}O]/[^{16}O]$. $\Delta^{17}O = \delta^{17}O - 0.516 \times \delta^{18}O$ and $\delta^{13}C$ and $\delta^{18}O$ are reported relative to VPDB and VSMOW, respectively. Δ_{47} is defined as the difference in ‰ between the measured R^{47} of the sample (principally $^{16}O^{13}C^{18}O/^{12}C^{16}O_2$ but also, to a lesser extent, $^{17}O^{12}C^{18}O/^{12}C^{16}O_2$ and $^{13}C^{17}O_2/^{12}C^{16}O_2$) and the R^{47} expected for that sample if its stable carbon and oxygen isotopes were randomly distributed among all CO_2 isotopologues (20).

Isotopic Analysis. $\delta^{13}C$, $\delta^{18}O$, and $\delta^{17}O$ of CO_2 were measured on a Finnigan MAT 252 isotope ratio mass spectrometer (IRMS) at the University of California, Berkeley. $\Delta^{17}O$ was measured by using the CeO_2 technique with a precision of ± 0.5‰ (44). Aliquots of the same CO_2 samples were analyzed for Δ_{47} by using a Finnigan MAT 253 IRMS at the California Institute of Technology configured to collect masses 44–49, inclusive, and standardized by comparison with CO_2 gases of known bulk isotopic composition that had been heated for 2 h at 1,000 °C to achieve a stochastic isotopic distribution (17). Masses 48 and 49 were used to detect residual hydrocarbon contamination. For Δ_{47} analysis, 12- to 18-μmol aliquots of SOLVE mission and Balloon CO_2 samples were purified of potential contaminants, such as hydrocarbons, by a pentane–liquid N_2 slush (−120 °C) as well as by passing them through a gas chromatographic (GC) column (Supleco Qplot, 530-μm i.d., 30-m length) at −20 °C, with column baking at 150 °C between samples (19, 45). All data were corrected for the presence of N_2O by using the method described previously (19). Each measurement consisted of 5–9 acquisitions (of 10 measurement cycles each), with typical standard deviations (acquisition-to-acquisition) of 0.06‰ in Δ_{47}. No evidence for organic contaminants was found when 1 representative CO_2 sample [20000131(30)1001] was tested (see SI).

Pulsed Photolysis Experiments. ^{18}O-labeled experiments were initiated with pulsed excimer laser photolysis (193 nm, 50- to 100-mJ pulse^{-1}, 1-Hz repetition rate, <200 pulses) of ≈1:100:3,000 static mixtures (100-Torr total pressure) of 97% $N_2{}^{18}O/CO_2$/He. For the 300 K experiments, a 15-cm-long stainless steel conflat chamber with quartz windows was used as a reaction chamber. Low-temperature experiments were performed in a 25-cm-long quartz chamber. $O(^1D)$ was produced by excimer laser photolysis of $N_2{}^{18}O$ at 193 nm (50- to 100-mJ pulse^{-1}). By using the absorption cross-section for N_2O at 193 nm (9×10^{-20} cm^2) (46) and a $O(^1D)$ quantum yield of 1, the total fraction of the CO_2 reservoir undergoing reaction was calculated to be <0.05%; we expect that reaction cycling was negligible. $N_2{}^{18}O$ was synthesized from the acid-catalyzed reduction of ^{18}O-labeled aqueous $NaNO_2$ (47), and its purity was assessed by using mass spectrometry and Fourier-transform infrared spectrometry.

Starting samples of CO_2 contained a stochastic distribution of isotopologues, generated in the manner described in the isotopic analysis section. The CO_2 isotopologue distribution was measured, and CO_2 was recollected cryogenically for use in the reaction chamber. The reaction chambers were baked overnight under vacuum before each experiment. Residence time in the reaction chamber had a negligible effect on Δ_{47} in the 300 K experiments, whereas the chamber cooling process was observed to enrich the starting material in $\delta^{18}O$ and Δ_{47}, by 0.5‰ and 0.13‰, respectively. These offset values were subtracted from final $\delta^{18}O$ and Δ_{47} values in 229 K experiments.

The reaction products were recollected cryogenically and purified in 2 GC steps. Separation of residual $N_2{}^{18}O$ and reacted CO_2 was achieved through a packed-column GC separation at 25 °C (PoraPak Q, 0.25 in o.d., 15-ft length, 30-mL min^{-1} He flow), after which the samples were purified with a capillary GC as described above. Because of the presence of $N_2{}^{18}O$ isobars with CO_2 at masses 46–49, mass 14 was also monitored to measure the extent of $N_2{}^{18}O$ contamination. Differences in mass 14 between the starting and product material of >5 mV (a variation typical of "clean" laboratory standards) were deemed contaminated and the data points rejected.

The difference between the initial and final $\delta^{18}O$ ($\Delta\delta^{18}O$) and Δ_{47} compositions was calculated assuming that $\delta^{13}C$ was unchanged, because there was no external carbon reservoir in the reaction. GC separation of $N_2{}^{18}O$ and CO_2 yielded a small, yet reproducible, Δ_{47} change of +0.13‰, which was present both when gases of stochastic isotope composition were analyzed and when aliquots of cylinder CO_2 working standard (Δ_{47} = 0.86‰) were analyzed. The source of this offset is likely a small amount of fractionation on the GC column, because it was relatively constant between experiments. Nevertheless, because of the apparent insensitivity of the Δ_{47} change to initial isotopic com-

position, the sample purification step was treated as a small additive effect on the measured Δ_{47}, with no effect on the overall kinetics measured.

A comprehensive, isotopologue-specific kinetics model of the $O(^1D)$-CO_2 photochemical experiment (144 isotope exchange reactions) was constructed in FACSIMILE. Statistical partitioning of isotope exchange products was used, as suggested by Yung (2) were used: Reactant $O(^1D)$ atoms had a 2/3 probability of isotope exchange, regardless of the isotope exchange reaction. The isotopic composition of the initial $O(^1D)$ was treated as a constant; for these ^{18}O-labeled experiments, ^{17}O and ^{16}O abundances were assumed to be negligible. Our determination of the $^{13}C/^{12}C$ KIE from this model also included a correction for the contribution of $^{17}O^{12}C^{18}O$ to the Δ_{47} signal.

Box Model for Estimating the Integrated Effective Midlatitude $O(^1D)$ Isotope Composition. The midlatitude $O(^1D)$ isotope composition was calculated by fitting the results of our laboratory photochemistry model to the slope of linear regressions (weighted by standard deviations) of the midlatitude Δ_{47} data. A quenching (Reaction **3a**) and nonquenching (Reaction **3b**) branching ratio of 9:1 in the isotope exchange reaction was used. Atmospheric Δ_{47} enrichments (e.g., $\Delta_{47} = 1.1‰$) were treated as $^{16}O^{13}C^{18}O$ enrichments exclusively, because contributions to Δ_{47} from $^{17}O^{12}C^{18}O$ and $^{13}C^{17}O_2$ are $\leq 3\%$. Uncertainties were estimated by varying $\Delta^{17}O$ and $\delta^{18}O$ to match the 2σ uncertainty in the slope of the weighted linear regressions. The upper and lower uncertainty limits of the reported $\Delta^{17}O$ and $\delta^{18}O$ values are correlated; they correspond to fits that simultaneously match the upper and lower uncertainty limits of the midlatitude Δ_{47} vs. $\Delta^{17}O$ and Δ_{47} vs. $\delta^{18}O$ weighted linear regressions.

Troposphere–Stratosphere–Mesosphere Mixing Model. The model contained 4 adjustable parameters to fit each high-latitude datum individually: mixing fractions and $\delta^{18}O$ values of stratospheric air and mesospheric air. Tropospheric isotopic compositions were fixed at typical clean surface troposphere values ($\delta^{13}C_{trop} = -8‰$, $\delta^{18}O_{trop} = 41‰$, $\delta^{17}O_{trop} = 21‰$, and $\Delta_{47trop} = 0.92‰$). We assumed oxygen isotope exchange was the dominant nonvortex process affecting CO_2 isotopologue distributions in the stratosphere, so the initial stratospheric mixing end-member composition was $\delta^{13}C_{strat} = -8‰$, $\Delta^{17}O_{strat} = 80.6‰$, $\delta^{18}O_{strat} = 98.0‰$, and $\Delta_{47strat} = 0$. Because of the uncertainty in our calculated $\Delta^{17}O_{strat}$ and $\delta^{18}O_{strat}$ values, however, $\delta^{18}O_{strat}$ was allowed to vary freely about our estimate above, and the modeled $\delta^{18}O_{strat}$ values generally fell within that range (see SI). The mesospheric CO_2 mixing endmember had an isotopic composition constrained by the calculations of Liang et al., namely $\delta^{17}O_{meso} = 0.3 \times \delta^{18}O_{meso}$. The multiply-substituted isotope distribution was fixed at $\Delta_{47meso} = 0$ for this simple mixing-only scenario because our kinetics experiments and the midlatitude stratosphere Δ_{47} values indicate that isotope exchange drives the isotopologue distribution toward a stochastic one. No measurements of mesospheric $\delta^{13}C$ exist, so $\delta^{13}C_{meso} = -8‰$ was used; however, the calculated enrichment in mesospheric $\delta^{18}O$ was insensitive to the choice of $\delta^{13}C$.

ACKNOWLEDGMENTS. We thank R. Lueb for WAS/CWAS field support and Y. L. Yung, G. A. Blake, and P. O. Wennberg for manuscript comments. This work was supported by the Davidow Fund (California Institute of Technology), the National Science Foundation, the National Aeronautics and Space Administration Upper Atmosphere Research Program, and the Camille Dreyfus Teacher–Scholar Award (to K.A.B.).

1. Yakir D (2003) The stable isotopic composition of atmospheric CO_2. *Treatise on Geochemistry*, eds Turekian KK, Holland HD (Elsevier, Amsterdam), Vol 4, pp 175–212.
2. Yung YL, Lee AYT, Irion FW, DeMore WB, Wen J (1997) Carbon dioxide in the atmosphere: Isotopic exchange with ozone and its use as a tracer in the middle atmosphere. *J Geophys Res* 102:10857–10866.
3. Ciais P, Meijer HAJ (1998) The $^{18}O/^{16}O$ isotope ratio of atmospheric CO_2 and its role in global carbon cycle research. *Stable Isotopes: Integration of Biological, Ecological and Geochemical Processes*, ed Griffiths H (BIOS Scientific, Oxford), pp 409–431.
4. Hoag KJ, Still CJ, Fung IY, Boering KA (2005) Triple oxygen isotope composition of tropospheric carbon dioxide as a tracer of terrestrial gross carbon fluxes. *Geophys Res Lett* 32:L02802.
5. Luz B, Barkan E, Bender ML, Thiemens MH, Boering KA (1999) Triple-isotope composition of atmospheric oxygen as a tracer of biosphere productivity. *Nature* 400:540–550.
6. Shaheen R, Janssen C, Röckmann T (2007) Investigations of the photochemical isotope equilibrium between O_2, CO_2, and O_3. *Atmos Chem Phys* 7:495–509.
7. Thiemens MH, Jackson T, Zipf EC, Erdman PW, van Egmond C (1995) Carbon dioxide and oxygen isotope anomalies in the mesosphere and stratosphere. *Science* 270:969–972.
8. Lämmerzahl P, Röckmann T, Brenninkmeijer CAM, Krankowsky D, Mauersberger K (2002) Oxygen isotope composition of stratospheric carbon dioxide. *Geophys Res Lett* 29:1582.
9. Bhattacharya SK, Savarino J, Thiemens MH (2000) A new class of oxygen isotopic fractionation in photodissociation of carbon dioxide: Potential implications for atmospheres of Mars and Earth. *Geophys Res Lett* 27:1459–1462.
10. Boering KA, et al. (2004) Observations of the anomalous oxygen isotopic composition of carbon dioxide in the lower stratosphere and the flux of the anomaly to the troposphere. *Geophys Res Lett* 31:L03109.
11. Kawagucci S, et al. (2008) Long-term observation of mass-independent oxygen isotope anomaly in stratospheric CO_2. *Atmos Chem Phys* 8:6189–6197.
12. Liang M-C, Blake GA, Yung YL (2008) Seasonal cycle of $C^{16}O^{16}O$, $C^{16}O^{17}O$, and $C^{16}O^{18}O$ in the middle atmosphere: Implications for mesospheric dynamics and biogeochemical sources and sinks of CO_2. *J Geophys Res Atmos* 113:D12305.
13. Wen J, Thiemens MH (1993) Multi-isotope study of the $O(^1D)+CO_2$ exchange and stratospheric consequences. *J Geophys Res* 98:12801–12808.
14. Johnston JC, Röckmann T, Brenninkmeijer CAM (2000) $CO_2 + O(^1D)$ isotopic exchange: Laboratory and modeling studies. *J Geophys Res* 105:15213–15229.
15. Chakraborty S, Bhattacharya SK (2003) Experimental investigation of oxygen isotope exchange between CO_2 and $O(^1D)$ and its relevance to the stratosphere. *J Geophys Res* 108:4724–4738.
16. Baulch DL, Breckenridge WH (1966) Isotopic exchange of $O(^1D)$ with carbon dioxide. *Trans Faraday Soc* 62:2768–2773.
17. Eiler JM, Schauble E (2004) $^{18}O^{13}C^{16}O$ in the Earth's atmosphere. *Geochim Cosmochim Acta* 68:4767–4777.
18. Affek HP, Xu X, Eiler JM (2007) Seasonal and diurnal variations of $^{18}O^{13}C^{16}O$ in air: Initial observations from Pasadena, CA. *Geochim Cosmochim Acta* 71:5033–5043.
19. Affek HP, Eiler JM (2006) Abundance of mass-47 CO_2 in urban air, car exhaust and human breath. *Geochim Cosmochim Acta* 70:1–12.
20. Eiler JM (2007) "Clumped-isotope" geochemistry—The study of naturally-occurring, multiply-substituted isotopologues. *Earth Planet Sci Lett* 262:309–327.
21. Newman PA, et al. (2002) An overview of the SOLVE/THESEO 2000 campaign. *J Geophys Res Atmos* 107:8259.
22. Greenblatt JB, et al. (2002) Defining the polar vortex edge from an N_2O:potential temperature correlation. *J Geophys Res Atmos* 107:8268.
23. Alexander B, Vollmer MK, Jackson T, Weiss RF, Thiemens MH (2001) Stratospheric CO_2 isotopic anomalies and SF_6 and CFC tracer concentrations in the Arctic polar vortex. *Geophys Res Lett* 28:4103–4106.
24. Liang M-C, Blake GA, Lewis BR, Yung YL (2007) Oxygen isotopic composition of carbon dioxide in the middle atmosphere. *Proc Natl Acad Sci USA* 104:21–25.
25. Perri MJ, Wyngarden ALV, Lin JJ, Lee YT, Boering KA (2004) Energy dependence of oxygen isotope exchange and quenching in the $O(^1D) + CO_2$ reaction: A crossed molecular beam study. *J Phys Chem A* 108:7995–8001.
26. Takahashi K, Taniguchi N, Sato Y, Matsumi Y (2002) Nonthermal steady state translational energy distributions of $O(^1D)$ in the stratosphere. *J Geophys Res* 107:4290–4296.
27. Mebel AM, Hayashi M, Kislov VV, Lin SH (2004) Theoretical study of oxygen isotope exchange and quenching in the $O(^1D) + CO_2$ reaction. *J Phys Chem A* 108:7983–7994.
28. Krankowsky D, et al. (2007) Stratospheric ozone isotope fractionations derived from collected samples. *J Geophys Res Atmos* 112:D08301.
29. Michalski G, Bhattacharya SK (2009) The role of symmetry in the mass independent isotope effect in ozone. *Proc Natl Acad Sci USA* 106:5493–5496.
30. Dylewski SM, Geiser JD, Houston PL (2001) The energy distribution, angular distribution, and alignment of the $O(^1D_2)$ fragment from the photodissociation of ozone between 235 and 305 nm. *J Chem Phys* 115:7460–7473.
31. Brenninkmeijer CAM, et al. (2003) Isotope effects in the chemistry of atmospheric trace compounds. *Chem Rev* 103:5125–5161.
32. Feilberg KL, D'Anna B, Johnson MS, Nielsen CJ (2005) Relative tropospheric photolysis rates of HCHO, $H^{13}CHO$, $HCH^{18}O$, and DCDO measured at the European photoreactor facility. *J Phys Chem A* 109:8314–8319.
33. Röckmann T, et al. (1998) Mass-independent oxygen isotope fractionation in atmospheric CO as a result of the reaction CO + OH. *Science* 281:544–546.
34. Feilberg KL, Johnson MS, Nielsen CJ (2005) Relative rates of reaction of $^{13}C^{16}O$, $^{12}C^{18}O$, $^{12}C^{17}O$ and $^{13}C^{18}O$ with OH and OD radicals. *Phys Chem Chem Phys* 7:2318–2323.
35. Feilberg KL, Johnson MS, Nielsen CJ (2004) Relative reaction rates of HCHO, HCDO, DCDO, $H^{13}CHO$, and $HCH^{18}O$ with OH, Cl, Br, and NO_3 radicals. *J Phys Chem A* 108:7393–7398.
36. Plumb RA, et al. (2003) Global tracer modeling during SOLVE: High-latitude descent and mixing. *J Geophys Res Atmos* 108:8309.
37. Ishidoya S, Sugawara S, Morimoto S, Aoki S, Nakazawa T (2008) Gravitational separation of major atmospheric components of nitrogen and oxygen in the stratosphere. *Geophys Res Lett* 35:L03811.
38. Craig H, Horibe Y, Sowers T (1988) Gravitational separation of gases and isotopes in polar ice caps. *Science* 242:1675–1678.
39. Wang Z, Schauble EA, Eiler JM (2004) Equilibrium thermodynamics of multiply substituted isotopologues of molecular gases. *Geochim Cosmochim Acta* 68:4779–4797.
40. Dash JG, Rempel AW, Wettlaufer JS (2006) The physics of premelted ice and its geophysical consequences. *Rev Mod Phys* 78:695–741.
41. Flocke F, et al. (1999) An examination of chemistry and transport processes in the tropical lower stratosphere using observations of long-lived and short-lived compounds obtained during STRAT and POLARIS. *J Geophys Res Atmos* 104:26625–26642.
42. Froidevaux L, et al. (2006) Early validation analyses of atmospheric profiles from EOS MLS on the Aura satellite. *IEEE Trans Geosci Remote Sens* 44:1106–1121.
43. Lueb RA, Ehhalt DH, Heidt LE (1975) Balloon-borne low temperature air sampler. *Rev Sci Instrum* 46:702–705.
44. Assonov SS, Brenninkmeijer CAM (2001) A new method to determine the ^{17}O isotopic abundance in CO_2 using oxygen isotope exchange with a solid oxide. *Rapid Commun Mass Spectrom* 15:2426–2437.
45. Ghosh P, et al. (2006) ^{13}C–^{18}O bonds in carbonate materials: A new kind of paleothermometer. *Geochim Cosmochim Acta* 70(6):1439–1456.
46. Sander SP, et al. (2006) *Chemical Kinetics and Photochemical Data for Use in Atmospheric Studies: Evaluation Number 15, JPL Publication 06-2* (Jet Propulsion Laboratory, Pasadena, CA).
47. McIlvin MR, Altabet MA (2005) Chemical conversion of nitrate and nitrite to nitrous oxide for nitrogen and oxygen isotopic analysis in freshwater and seawater. *Anal Chem* 77:5589–5595.